


 Cite this: *Lab Chip*, 2019, 19, 524

An integrated droplet-digital microfluidic system for on-demand droplet creation, mixing, incubation, and sorting†

 Fatemeh Ahmadi, ^{ab} Kenza Samlali, ^{ab}
Philippe Q. N. Vo ^{ab} and Steve C. C. Shih ^{*abc}

Droplet microfluidics is a technique that has the ability to compartmentalize reactions in sub nano- (or pico-) liter volumes that can potentially enable millions of distinct biological assays to be performed on individual cells. In a typical droplet microfluidic system, droplets are manipulated by pressure-based flows. This has limited the fluidic operations that can be performed in these devices. Digital microfluidics is an alternative microfluidic paradigm with precise control and manipulation over individual droplets. Here, we implement an integrated droplet-digital microfluidic (which we call 'ID2M') system in which common fluidic operations (*i.e.* droplet generation, cell encapsulation, droplet merging and mixing, droplet trapping and incubation, and droplet sorting) can be performed. With the addition of electrodes, we have been able to create droplets on-demand, tune their volumes on-demand, and merge and mix several droplets to produce a dilution series. Moreover, this device can trap and incubate droplets for 24 h that can consequently be sorted and analyzed in multiple *n*-ary channels (as opposed to typical binary channels). The ID2M platform has been validated as a robust on-demand screening system by sorting fluorescein droplets of different concentration with an efficiency of ~96%. The utility of the new system is further demonstrated by culturing and sorting tolerant yeast mutants and wild-type yeast cells in ionic liquid based on their growth profiles. This new platform for both droplet and digital microfluidics has the potential to be used for screening different conditions on-chip and for applications like directed evolution.

 Received 29th October 2018,
Accepted 30th December 2018

DOI: 10.1039/c8lc01170b

rsc.li/loc

Introduction

Droplet microfluidics involves monodisperse aqueous droplets that are generated by a pressure-driven flow in a continuous oil phase where droplets are typically analysed and manipulated at very high rates (>1000 droplets per second). The use of droplet microfluidic technology has enabled a wide variety of applications, specifically in the area of high-throughput chemistry and biology.^{1–4} This two-phase microfluidic format can undergo a number of different fluidic operations – droplet generation, encapsulation, mixing, and sorting. Sorting is in particular an important operation that allows selection of subpopulation of cells, DNA, and biomolecules in the droplets.^{5–7} A variety of sorting methods have been shown in the literature using dielectrophoresis, mag-

netic, thermal, or acoustic methods^{8–11} (for more extensive review please see ref. 12). Each of these have their own advantages in terms of speed, reliability and ease of implementation. However, typical sorting methods are usually based only on binary sorting – *i.e.* sorting droplets that are based on two levels of output – which can limit the range of detecting rare events and to sort based on different constituents in the droplet (*e.g.*, multiple concentrations of an additive).

There is an alternative type of microfluidics that enables on-demand droplet control called digital microfluidics.^{13,14} This platform allows manipulation of discrete droplets by electrostatic forces on an array of electrodes coated with an insulating dielectric. One of the main advantages of DMF is it facilitates precise control over many different reagents simultaneously and independently by application of potentials (or by acoustic and contactless methods^{15–17}). This has enabled DMF to be a well-suited platform to carry out many different types of applications, namely, cell-based assays,^{18,19} synthetic biology,^{20,21} and point-of-care diagnostics.^{22,23} Most of these types of applications are configured in a two-plate format, in which droplets are manipulated between a top and bottom substrate bearing a ground and driving electrodes

^a Department of Electrical and Computer Engineering, Concordia University, Montréal, Québec, Canada. E-mail: steve.shih@concordia.ca;
Tel: +1 514 848 2424x7579

^b Centre for Applied Synthetic Biology, Concordia University, Montréal, Québec, Canada

^c Department of Biology, Concordia University, Montréal, Québec, Canada

† Electronic supplementary information (ESI) available. See DOI: 10.1039/c8lc01170b

respectively. There is another digital microfluidic configuration in which droplets are actuated on a single substrate with co-planar configuration of electrodes. Although in this configuration droplets lack the capacity to dispense, this format does allow better mixing which is useful in applications carrying out chemical reactions.^{24,25} Likewise, it may be useful to couple single-plate DMF with microchannels as a chemical pre-processing unit without the need for pre-column reactions since DMF can rapidly mix different analytes in seconds and separated using the channels.^{26,27} The idea of integrating DMF with other microfluidic paradigms is an exciting innovation as it combines advantages of both systems while minimizing the disadvantages of the individual systems.

The work reported here combines the use of single-plate DMF and droplet-in-channel microfluidics. Our work joins a group of studies that have used digital microfluidics and combined it with other microfluidic paradigms.^{21,26–32} In most of these studies, DMF was integrated with microchannels and is used to control bulk fluid flow or for pre-separation of chemical reactions. There is one group (to our knowledge) that have implemented DMF with droplets-in-channel microfluidics. From the Mugele group,^{30–32} they have discussed a series of studies that discusses the physical phenomenon behind the integration of electrowetting with microfluidics to control the size and frequency of drop formation and the binary sorting of droplets. We present a method that includes several advances relative to the methods described by Mugele *et al.*,^{30–32} including the integration of on-demand droplet generation with n-ary sorting (as opposed to binary³³) on the same device (which we call integrated digital-droplet microfluidic – ID2M). Furthermore, additional advancements of the device include other important and essential operations for typical droplet-based microfluidic assays. (1) On-demand droplet mixing enabling control and creation of different concentration of droplets. Typical droplet-in-channel techniques have depended on fusion³⁴ or picoinjection³⁵ methods for mixing but these techniques only allow one reagent addition to an existing droplet and require exquisite control over flow rates, timing, and fluidic resistance. Our integrated device can create a range of different concentrations with multiple additions of reagent droplets by application of an electric potential without any consideration for other parameters (*e.g.*, timing). (2) We also include areas to trap and to incubate droplets for 24 h. To date, this operation has not been shown on such a device and does not require delay lines^{36,37} or on- and off-chip reservoirs for incubation.^{38,39} Finally, we show the utility of our system by applying it to a biological study (instead of manipulation of water and oil^{30–32}) that examines mutant and wild-type yeast cells under ionic liquid conditions which can be useful for applications related to biofuel production. We believe this is an important step in the field of digital and droplet microfluidics as this can possibly enable more control for droplet microfluidic devices while increase droplet throughput for digital microfluidic devices.

Materials and methods

Reagents and materials

1-Ethyl-3-methylimidazolium acetate $\geq 95\%$ (HPLC grade), ethyl methanesulfonate, sodium thiosulfate, sodium hydroxide (lab grade), fluorescein (free acid) dye content 95%, yeast nitrogen base without amino acids and with ammonium sulfate, bovine serum albumin (lyophilized powder) $\geq 96\%$, and α -D-glucose anhydrous 96% were purchased from Sigma (Oakville, ON Canada), unless specified otherwise. L-Leucine, L-histidine, L-methionine, and uracil were purchased from Bio Basic Canada Inc. Yeast BY4741 strain (genotype: MATa his3 Δ 1 leu2 Δ 0 met15 Δ 0 ura3 Δ 0) was generously donated from Dr. Vincent Martin. 3M Novec HFE7500 engineering fluid was purchased from M.G. Chemicals (Burlington, ON Canada). Aquapel™ was purchased from Aquapel.ca (Lachute, QC Canada). 20 g of 5% wt of fluoro-surfactant dissolved in HFE7500 was purchased from Ran Biotechnologies (Beverly, MA). Sodium phosphate monobasic and sodium phosphate dibasic (anhydrous, ACS grade) were purchased from BioShop (Burlington, ON).

Photolithography reagents and supplies included chromium coated with S1811 photoresist on glass slides from Telic (Valencia, CA), MF-321 positive photoresist developer from Rohm and Haas (Marlborough, MA), CR-4 chromium etchant from OM Group (Cleveland, OH), and AZ-300T photoresist stripper from AZ Electronic Materials (Somerville, NJ). Polylactic acid (PLA) material for 3D printing was purchased from 3Dshop (Mississauga, ON, Canada). Poly(dimethylsiloxane) (PDMS – Sylgard 194) was purchased from Krayden Inc. (Westminster, CO). SU8 photoresist and developer were purchased from Microchem (Westborough, MA). De-ionized (DI) water had a resistivity of 18 M Ω cm at 25 °C.

A 100 mM sodium phosphate buffer (SPB) was prepared by mixing 5.77 mL of 1 M Na₂HPO₄ and 4.23 mL of 1 M NaH₂PO₄ solutions (pH 7.0). 5 g of sodium thiosulfate salt was added to deionized water to produce a 5% (w/v) sodium thiosulfate (STS) solution. Fluorescein solutions (0.5 mM) was prepared by adding 1.66 mg of fluorescein powder (332.3 g mol⁻¹) to 10 mL 1 M NaOH solution that was made by adding 0.4 g NaOH to 10 mL DI water.

Device fabrication and operation

ID2M device masks were designed using AutoCAD 2016 and a transparent photomask was printed by CAD/Art Services Inc. (Bandon, OR). The ID2M microfluidic chip consisted of three layers: a digital microfluidic, dielectric, and channel layer (Fig. 1a). As described previously,^{20,40} electrodes were patterned on a glass substrate with chromium and coated with positive photoresist S1811, by UV exposure (5 s) on a Quintel Q-4000 mask aligner (Neutronix Quintel, Morgan Hill, CA). Exposed substrates were developed in Microposit MF-321 developer (2 min), rinsed with DI water, and post-baked on a hot plate (115 °C, 1 min). Substrates were etched in chromium (CR-4) etchant (2 min). Remaining photoresist was stripped in AZ300T (2 min). DMF devices were rinsed by

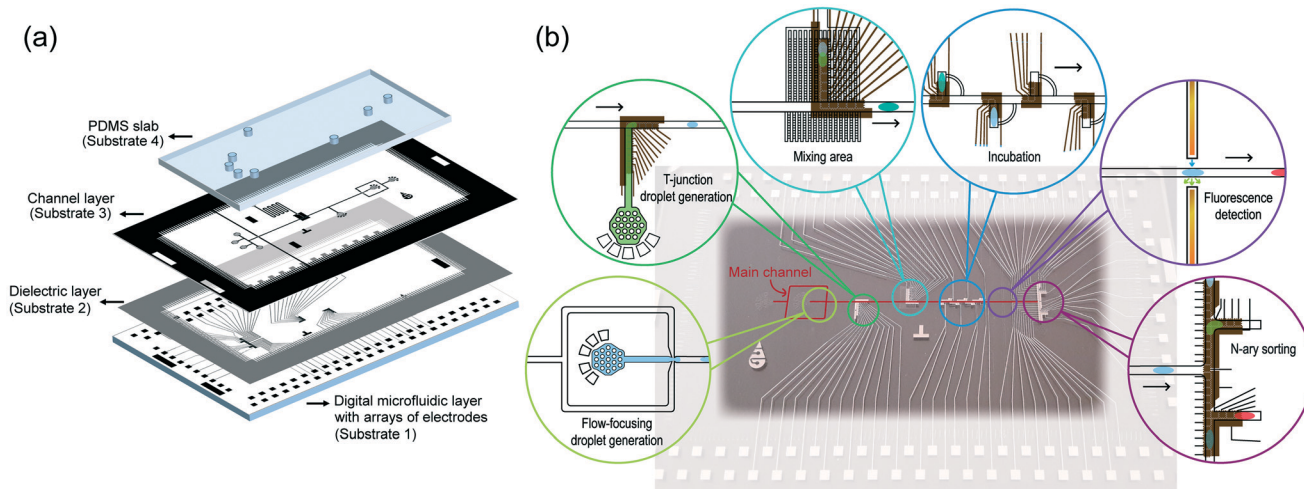


Fig. 1 ID2M microfluidic device. (a) Exploded view of the ID2M microfluidic device. The bottom layer is the digital microfluidic (DMF) configuration which is covered with a dielectric SU-8 layer $\sim 7 \mu\text{m}$ thickness. The channel layer is $300 \mu\text{m}$ wide and $110\text{--}120 \mu\text{m}$ high and is fabricated on top of the bottom layer. A PDMS slab of thickness $\sim 5 \text{ mm}$ was bonded to seal the channel layer. (b) A photo of the device with schematics depicting the operations of the device, namely droplet dispensing (using T-junction and flow focusing), droplet mixing, droplet incubation, droplet detection, and droplet n-ary sorting. Highlighted in red shows the main channel on the device in which droplets are transported from one region to another. Mixing area contains sinking channels to reduce the oil flow rate.

acetone, isopropanol (IPA), and DI water. The device surface was treated with a plasma cleaner (Harrick Plasma PDC-001, Ithaca, NY) for 2 min and then immediately spin-coated (Laurell, North Wales, PA) with $7 \mu\text{m}$ SU8-5 photoresist (10 s, 500 rpm, 30 s 2000 rpm). SU-8 5 was soft-baked (1. $65 \text{ }^\circ\text{C}$, 2 min, 2. $95 \text{ }^\circ\text{C}$, 5 min) and exposed to UV light (5 s) under the dielectric mask. Post-exposure bake (1. $65 \text{ }^\circ\text{C}$, 1 min, 2. $95 \text{ }^\circ\text{C}$, 1 min) was followed by immersing in SU-8 developer (2 min). Substrates are rinsed with IPA and DI water, a hard bake was performed in three steps (1. $65 \text{ }^\circ\text{C}$, 2 min, 2. $95 \text{ }^\circ\text{C}$, 4 min, 3. $180 \text{ }^\circ\text{C}$, 10 min). For the channel layer, devices were cleaned again with IPA and DI water prior to plasma cleaning (2 min). Next, SU-8 2075 photoresist was immediately spin-coated (1. 10 s 500 rpm, 2. 30 s 2000 rpm) on the chip as a $110\text{--}120 \mu\text{m}$ third layer, and soft-baked ($65 \text{ }^\circ\text{C}$, 3 min; $95 \text{ }^\circ\text{C}$, 9 min). Following UV exposure (15 s), devices were post-baked (1. $65 \text{ }^\circ\text{C}$, 2 min–2. $95 \text{ }^\circ\text{C}$, 7 min), developed in SU-8 developer (7 min) and rinsed with IPA and DI water. The devices were hard-baked (1. $65 \text{ }^\circ\text{C}$, 2 min, 2. $95 \text{ }^\circ\text{C}$, 4 min, 3. $180 \text{ }^\circ\text{C}$, 10 min). The integrated microfluidic chip was bonded to a slab ($60 \text{ mm} \times 30 \text{ mm}$) of $\sim 0.5 \text{ mm}$ thick PDMS (1:10 weight ratio, w/w curing agent to prepolymer, cured at $65 \text{ }^\circ\text{C}$ for 3 hours). Inlets and outlets were created using a 0.75 mm puncher (Biopsy Punch, Sklar, West Chester, PA). Before bonding, the PDMS slab was plasma-treated for $\sim 1 \text{ min}$ and exposed to (3-aminopropyl)triethoxysilane 99% in a desiccator for 30 min. PDMS was immediately bonded to the device and baked at $160 \text{ }^\circ\text{C}$ for 20 min. Before operation, channels were treated with AquapelTM for $\sim 5 \text{ min}$ and rinsed with HFE oil mixed with 0.75% fluorosurfactant. Syringes were prepared with the following fittings and tubing: 1/4-28 to 10-32 PEEK adapter, (10-32) peek union assembly, finger tight micro ferrule 10-32 coned for 1/32" OD, and PEEK

tubing (1/32" diameter) from IDEX Health & Science, LLC (Oak Harbor, WA). Gastight glass $500 \mu\text{L}$ -syringes were purchased from Hamilton (Reno, NV) and installed on the neMESYS system (Cetoni, Korbussen, DE).

Device operation comprised of five stages: droplet generation by a flow-focusing or T-junction configuration followed by droplet mixing, incubation, detection, and sorting. Droplet generation by flow-focusing was implemented by initializing the flow rates using the neMESYS for the aqueous and oil flow rates to $0.0005 [\mu\text{L s}^{-1}]$ and $0.01 [\mu\text{L s}^{-1}]$ respectively. For the T-junction configuration, droplets were created on-demand by four steps: (1) the aqueous flow was initialized at $0.0005 [\mu\text{L s}^{-1}]$, (2) when the aqueous flow reaches the sixth electrode, an AC voltage (15 kHz, $200 \text{ V}_{\text{rms}}$) was used to drive the flow to the T-junction, (3) two electrodes were sequentially actuated (*i.e.* electrodes are turned on and off) to drag the fluid to the main channel (shown in red; Fig. 1b) and (4) a $\sim 30 \text{ nL}$ droplet is formed by both intersecting the oil phase with flow rate of $0.01 [\mu\text{L s}^{-1}]$ and turning on electrodes in the T-junction and main channel as shown in Fig. S1.† After on-demand droplet generation, droplets were pressure-driven using the oil phase in the main channel and using actuation sequences to drive the droplet into the mixing region (15 kHz, $200 \text{ V}_{\text{rms}}$, under oil flowrate of $0.01 \mu\text{L s}^{-1}$). Droplets were mixed by actuating underlying electrodes and the mixed droplet was actuated to the main channel. For incubation, droplets were directed to the traps actuating the designated electrodes. After incubation, droplets pass through a detection region which were further sorted by actuation of the electrodes. For droplet size calculations, images of the droplets were acquired and uploaded into ImageJ (National Institute of Health, USA). An imaging pipeline was created to calculate the droplet volume based on an ellipsoid volume formula given that the droplet height was set to $110 \mu\text{m}$.

ID2M microfluidic optical fiber detection interface

The optical fiber detection interface consists of a Flame spectrometer (Ocean Optics, Largo, FL), two bare fiber (100 μm core) with numerical aperture of 0.22, and a multi-channel LED light sources that contains four high-power (1 mW) LED modules: 470, 530, 590, 627 nm. Two optical fibers were inserted into two fabricated 300 μm channels that were perpendicular to the direction of the fluid flow (see Fig. 1b). One fiber was connected to the multi-channel LED source, while the other was connected to the Flame spectrometer. The fiber ends were polished carefully using the ocean optics termination kit and fitted with an SMA connector by the help of bare boots for guiding the bare fiber. The distance between the fiber and the channel is ~ 200 μm . All data were collected using the Ocean View spectroscopy software (Ocean Optics, Largo, FL) using the following settings: (a) for fluorescence detection: integration time 100 ms, boxcar smoothing width = 3, number of scans = 5, update rate = 1. Strip chart was enabled to collect data from a single wavelength (530 nm) and executed without stopping. (b) for absorbance detection: same setting with boxcar smoothing width = 2, number of scans = 2.

On-chip calibration curves – fluorescein measurement

A droplet containing fluorescein (1 mM each in 1 M NaOH buffer, pH 9) was generated using the flow-focusing configuration with fluorescein ($0.0005 \mu\text{L s}^{-1}$) and HFE oil ($0.01 \mu\text{L s}^{-1}$). A droplet of buffer or water (~ 30 nL) was generated using the on-demand T-junction configuration. The droplets were merged and mixed by actuation of underlying electrodes. The amount of buffer droplets added to one fluorescein droplet created four different concentrations: 1, 0.5, 0.25, and 0.125 mM. After mixing, droplets were detected by using our optical fiber setup, and sorted by actuating a sorting sequence for one of the four different on-demand sorting channels. Peak intensities were recorded for each concentration with time traces of the recorded signals. The standard deviation was calculated from 20 replicates.

EMS mutagenesis and generating ionic liquid resistant yeast strains

Before generating the mutant library, wild-type *S. cerevisiae* BY4741 yeast cells were stored on agar plates containing synthetic defined medium (6.8 yeast nitrogen base without amino acids, 20 g agar, 20 g 2% glucose, 20 g methionine, 20 g histidine, 20 g uracil, 120 g leucine) at 4 °C. Wild-type yeast was grown in 50 mL of synthetic defined medium (30 °C, 200 rpm) for 48 hours. Aliquots of 2×10^8 yeast cells (O.D. ~ 1) were transferred to four micro-centrifuge tubes corresponding to technical triplicate and one control sample. The cells were washed two times with phosphate buffered saline (PBS) and a single time with sodium phosphate buffer (SPB) (0.1 M – pH 7.0). After centrifugation, the pellets were re-suspended in 1.5 mL SPB. For mutagenesis, cells were exposed to ethyl methanesulfonate (EMS) according to Winston's protocol.⁴¹

To generate a standard curve for viability after EMS mutagenesis, our 15 mL Falcon tubes (corresponding to three different EMS treatment time) were filled with 1 mL SPB and 0.7 mL cell solution of each micro-centrifuge tube. 50 μL of EMS was added to three of the 15 mL falcon tubes in a biological safety cabinet. The control sample (*i.e.* wild-type cells) were kept without EMS addition. All tubes were incubated at 30 °C on a shaker (200 rpm) for 30 min. Cells were exposed to EMS for 40, 50, 60, 75, and 90 min. Mutagenesis was stopped by adding 8 mL of 5% (w/v) sterile sodium thiosulfate (STS) solution at each time point. Aliquots of each falcon tubes diluted in SD media were plated on solid SD media. Plates were incubated at 30 °C for 48 h. Cell viability was measured by comparing colony formation of each EMS time point and the wild-type cells (Fig. S2†).

To generate 1-ethyl-3-methylimidazolium acetate IL resistant cells, the mutagenesis is repeated for 60, 75, and 90 min. Resulting aliquots were inoculated in 5 mL synthetic defined medium for 24 h at 30 °C on a shaker with 200 rpm. Next, the mutants were inoculated in 5 mL synthetic defined medium and 50, 75, or 100 mM 1-ethyl-3-methylimidazolium acetate IL and incubated for 24 h at 30 °C on a shaker with 200 rpm. 1 mL aliquots of each test tubes along with a wild-type sample were diluted 100 times with SD media and then were plated onto several solid SD plates containing 50, 75, or 100 mM IL. These plates were incubated for 4–6 days at 30 °C. Colonies were randomly selected from the plates and cultured in 5 mL SD media at 30 °C. After 24 h, we measured the OD of the culture and if the OD was greater than 0.3, samples were diluted and cultured in different ionic liquid conditions otherwise they were discarded. If selected, an aliquot (depending on IL concentration) from the 5 mL culture was added to the wells of a microwell plate to make up a final volume of 200 μL . In each well, the OD was measured every 20 min at 30 °C with shaking at 200 rpm for 48 hours using a Tecan Sunrise microplate reader (Tecan, Salzburg, Austria) with the following settings (measurement wavelength: 595 nm). Three replicates were measured for each condition.

N-ary sorting of yeast mutant library on ID2M device

For analyzing the effect of IL on wild-type and mutant yeast on chip, the two fastest growing IL tolerant mutants and wild-type yeast were cultured in SD without IL for 48 h. A 500 μL syringe was prepared with a cell suspension of 2×10^5 cells per mL in SD media containing 1% bovine serum albumin (BSA) and a syringe containing HFE oil with 2% fluorinated surfactant. Both syringes were connected to the inlets of the device using PEEK tubing (1/32 inch diameter). Cell encapsulation was performed through flow focusing (using Poisson statistics) with flow rates of $0.0008 \mu\text{L s}^{-1}$ and $0.01 \mu\text{L s}^{-1}$ for cells and oil, respectively to generate a droplet with volume of ~ 35 nL. For the T-junction droplet generator, a syringe was filled with 200 mM IL and ~ 35 nL droplets were formed on demand. Droplets containing a single cell were

actuated into the mixing region by sequentially applying 200 V_{RMS} (15 kHz) to the electrodes. The droplet was merged with an on-demand generated droplet of IL and mixed by moving the droplet back-and-forth along the linear path. Upon mixing the droplet with a 200 mM IL, the mixed droplet of cells and IL (with a final concentration of 100 mM IL) was actuated to the main channel and was trapped into incubation slot using actuation. This process was repeated for three other incubation regions. After trapping all four droplets, the ID2M device was removed from the automation system and droplets were incubated for 24 h at 30 °C in a humidified chamber.

After incubation, droplets were actuated to the main channel and passed through the optical detection area where the two optical fibers were placed perpendicular to the main channel. According to the absorbance peaks differences, droplets were sorted into three groups using the three sorting channels. Any excess droplets in this procedure was actuated to the waste channel. During all droplet operation procedures (*i.e.* mixing, trapping, incubation, sorting) and when droplets were in the main channel, oil flow rates were maintained at 0.01 $\mu\text{L s}^{-1}$. Typically, after three replicate experiments on the same device, the devices were re-treated with Aquapel™ for ~5 min and rinsed with HFE oil mixed with 0.75% fluorosurfactant.

COMSOL simulation

We conducted a simulation of the mixing area with the sinking channels, using COMSOL Multiphysics V5.3 (COMSOL Inc., Cambridge, MA, USA). Parameters are shown in Table 1 and following assumptions were made for simplification: 1) Newtonian fluid, 2) no-slip boundary condition, and 3) incompressible flow. A single-phase laminar flow using Navier Stokes model was selected as the physics of our stationary study with the assumption that our fluid is 3M™ Novec™ 7100 Engineered Fluid. Wall boundaries and inlet and outlet were defined as depicted in Fig. S3.† The inlet velocity of the fluid flow was initialized to 0.033 m s^{-1} .

Results and discussion

Device characterization and optimization

We have developed a new microfluidics architecture called ID2M, merging droplet microfluidics (useful for generating and sorting droplets) with digital microfluidics (useful for on-demand droplet manipulation and individual control of droplets). The ID2M device were formed by creating a single-plate DMF device (*i.e.* the ground and driving electrodes are

co-planar) and fabricating a network of channels on top, with inlets and outlets for generating and sorting droplets respectively, and an area for droplet mixing. An exploded view (Fig. 1a) shows the digital microfluidic device as the bottom substrate with 104 patterned electrodes, the dielectric layer (substrate 1 and 2), the network of channels patterned in SU-8 photoresist, and a slab of PDMS with inlets and outlets (substrates 3 and 4). This multilayer integrated architecture facilitates pressure-based and on-demand droplet generation using flow focusing and T-junction configurations respectively, on-demand droplet mixing, on-demand droplet trapping and incubation, and on-demand droplet sorting. The combined multilayer architecture represents a significant advance over other types droplet-to-digital methods which relies on two separate design configurations which can cause difficulties in moving the droplet from one platform to the other as reported previously.^{21,26–28}

Droplets in the main channel are moved by pressure flow and electrical potentials move droplets to the mixing, incubation, and sorting regions (*i.e.* away from the main channel) with throughput of ~1 Hz (Fig. 1b). A central feature of this design is that droplets in the main channel can be moved to the mixing area to merge with other droplets. For example, a droplet containing dilution buffer is generated on-demand *via* actuation from the T-junction, then actuated to the mixing area, and merged and mixed with other droplets in the main channel. This process can be repeated to create of a diluent series of droplets. After generating the diluent droplet, these droplets can be actuated to the main channel and can be incubated in the trap and sorted in one of the channels (after incubation) using electrostatic actuation. Typical droplet microfluidic systems use electrocoalescence^{42,43} or picoinjection^{35,44} techniques to sequentially add reagents to droplets at different times. However, these techniques, as of yet, have not demonstrated the generation of a dilution series of droplets. In addition to generation of a diluent series of droplets, the droplets are capable to be sorted in four different channels. The device allows for droplet samples to be sorted by multiple conditions based on a larger gradient, like multiple levels of fluorescence and absorbance, instead of typical binary sorters. This suggests that using a system (such as ID2M) can provide direct droplet control that enables generation of a droplet dilution series and droplet sorting in multiple fractions for droplet microfluidic systems.

Electrode shape and design are important parameters to ensure high-fidelity droplet movement on the device (Fig. 1b). In initial electrode designs, we followed an one electrode design on the bottom plate with alternating ground and driving potentials.^{31,45} However, droplets in the main channel were not able to overcome the pressure generated from the oil flow rate and could not be actuated into the mixing, incubation, or different sorting regions. A coplanar electrode configuration (*i.e.* with adjacent ground and actuated electrodes on the same plane), as shown by some groups,^{46–48} showed optimal droplet manipulation. The introduction of a ground electrode (or grounding line) on the

Table 1 COMSOL simulation parameters used for modeling the sinking channels in the mixing area

Parameter	Value	Unit
Oil density (ρ)	1614	kg m^{-3}
Dynamic viscosity (μ)	0.00124	Pa s
Inlet velocity (u_0)	0.0003	m s^{-1}

same plane may not generate the highest applied force as compared to other electrode designs,⁴⁶ but the selected design is easiest to fabricate and is capable to overcome the applied pressure on the droplet in our system (oil flow rate of 0.005–0.05 $\mu\text{L s}^{-1}$).

The fabrication protocol for the ID2M devices needed to be optimized to ensure strong adhesion of the dielectric, channel, and PDMS layers during fabrication, and to allow droplets to be controlled by application of electric potentials in the mixing area. For the former challenge, we found that introducing 300 μm spaced repeated finger-like structures on the boundary of the dielectric layer increases adhesion to the substrate (Fig. S4†). Layers that did not have these finger-like structures or if the repeated finger like structures are spaced far apart ($>500 \mu\text{m}$), SU-8 5 tends to peel or crack easily. We hypothesize these cracks are mostly made by internal stresses as high evaporation and heating/cooling rate in addition to temperature differences in different layers of SU-8 5 causes residual stresses in the layer.⁴⁹ To increase the adhesion of the PDMS slab to the SU-8 layer, we used (3-aminopropyl)triethoxysilane (APTES)⁵⁰ vapor deposition after plasma treatment of the PDMS, the slab were exposed to the vapor of APTES in a desiccator for 30 min forming aminosilane molecule on the surface of the PDMS. This surface favorably reacts with the epoxy group from the SU-8 surface which strengthens the bond between the PDMS and SU-8 layer.

To slow down the flow rate and to enable droplets to be actuated from the main channel to the mixing area, we added sinking channels in the mixing area. We added multiple sink channels⁵¹ to create flow eddies from the main flow channel which allow the oil phase to have multiple flow paths (Fig. 1b and S5†). The reduction in oil flow rate enables droplets in the main channel to be actuated into the mixing channel. In our initial designs, we created a side channel (*i.e.* a channel branching out of the main channel) with the coplanar electrodes; however, droplets were not capable to be moved by actuation from the main channel to the mixing area. We explored increasing the voltage;⁵² however the higher voltage tend to cause dielectric breakdown in the oil phase and cause droplet breakup which created small satellite droplets. The sink channels are particularly important when a droplet is already in the mixing area since the droplet acts as a plug (*i.e.* increasing the hydrodynamic resistance).⁵³ Since the hydrodynamic resistance in the mixing channel is higher than the main channel when a droplet is present, the generated droplets favour flow in the main channel. Alternatively, having multiple sink channels creates multiple flow paths (*i.e.* reducing the resistance in the mixing channel), leading to mixing of the droplets in this area.

An additional component for successful device operation was optimization of the configuration of the n-ary sorting channels. We initially tested with Y-shaped configuration,^{5,54} in which droplets are discriminated by two (or more^{9,55,56}) physical characteristics. However, the Y-channels have a tendency to create a stagnation zone (*i.e.* an area where the

droplet faces an uncontrolled choice for an outlet) even with the additional bias of the electric potentials. The additional bias also creates an asymmetric presence of drops (creating different resistances) when it is expanded to more than two channels.³³ Instead, we designed a symmetrical T-channel that consists of four different sorting areas with similar resistances. Pressure-driven droplets are detected using the optical interface and are biased directly to a channel by actuation. In the future, we may design rails⁵⁷ or linear electrodes⁵⁸ with the symmetric T-channels to reduce the footprint and to increase the number of sorting channels.

On-demand droplet generation, mixing, incubation, and sorting

The unique system that we have reported here enables integration of a variety of fluidic manipulations steps such as on-demand droplet generation, merging and mixing, and n-ary sorting. As shown in Fig. 2a (also see ESI† video), droplets can be generated through flow-focusing geometry (1–10 kHz) or by on-demand generation using T-junction (frame i, ii, and iii), stored (frame iv and v), merged and mixed (frame vi), incubated (frame vii), and sorted (frame viii and ix) with throughput of $\sim 1 \text{ Hz}$. The device can generate droplets on-demand by using a T-junction configuration which combines the pressure of the continuous oil phase and electrostatic actuation of the aqueous flow. As shown in Fig. 2b, the droplet volume generated by the T-junction can be tuned by only changing the oil flow rate (as opposed to tuning both aqueous and oil flows)^{59,60} and using actuation to move the aqueous flow. This setup enabled a wide range of volumes being generated (40–115 nL) by tuning the oil flow between 0.001 and 0.06 $\mu\text{L s}^{-1}$. As a comparison, we generated droplets hydrodynamically by changing the oil flow rate (while keeping the aqueous flow rate constant) which resulted in minimal changes in the volume when increasing the oil flow rate $>0.01 \mu\text{L s}^{-1}$. We hypothesize that traditional systems for tuning droplet sizes is limited by the orifice size and the relative strength of interfacial tension and hydrodynamic shear forces,³⁶ which can be alleviated using on-demand droplet generation. In addition to on-demand droplet generation, mixing and sorting are particularly useful capabilities, as most droplet microfluidic systems are incapable of generating dilutions of droplets and sorting them into multiple channels. In the design reported here, after droplet generation, droplets can be actuated to the mixing area and merged with another droplet (Fig. 2a, frame iv–vi) and transferred to the main channel area for sorting and analysis (Fig. 2a, frame vii–ix). To illustrate this, we used this method to generate calibration standards on this platform with sorting analysis.

Dilutions were formed by merging a droplet containing analyte (fluorescein) with a droplet of diluent (buffer). This merged droplet was mixed (by moving the merged droplet in a linear pattern – up-and-down – for several seconds⁶¹) producing a droplet with a $2\times$ dilution of analyte. This droplet

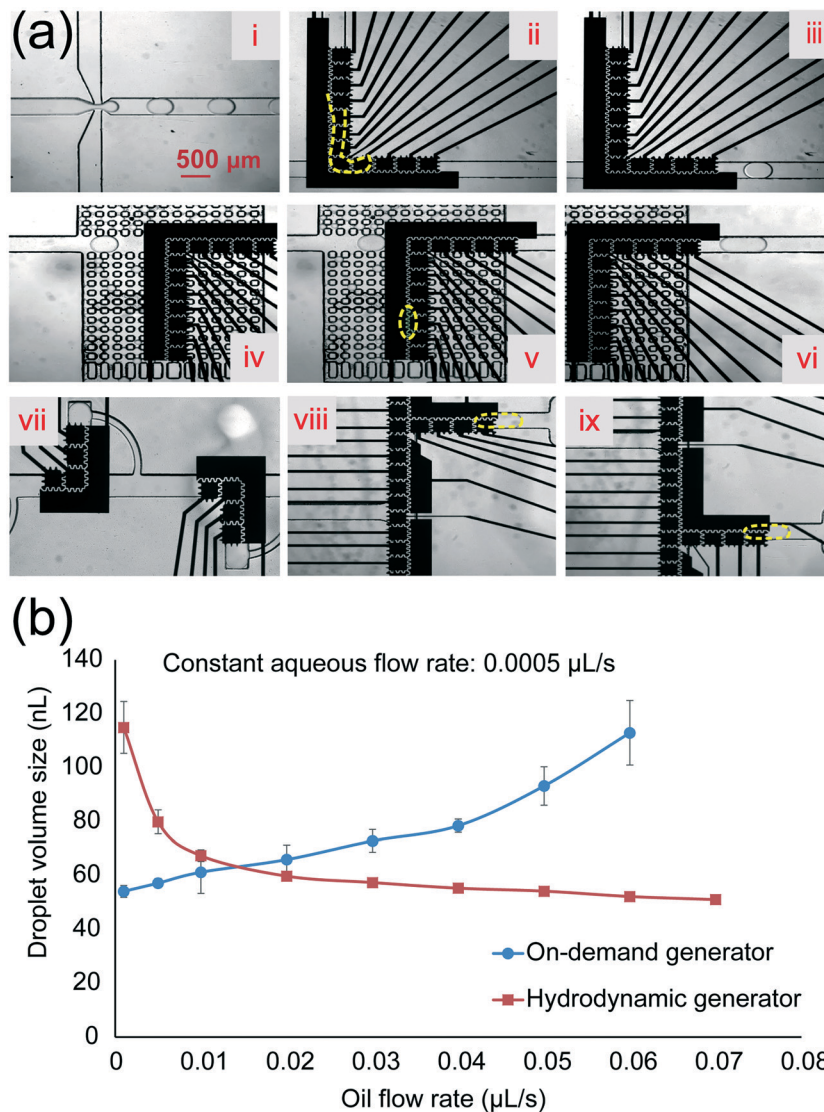


Fig. 2 ID2M droplet operations. (a) Series of images from a movie (top-view) depicting the droplet operations on a device. Frames i–iii illustrate droplet generation from flow-focusing and on-demand (T-junction) techniques, and frames iv–vi subsequent merging and mixing of droplets. Frames vii show droplet incubation (for incubating cells and other constituents) and frames viii and ix show droplet sorting in four different channels. Fluids and droplets are highlighted for visual clarity. (b) Droplet size as a function of oil flow rate at a constant water flow rate ($0.0005 \mu\text{L s}^{-1}$) using flow-focusing and T-junction (on-demand) configurations. Each point represents eight droplets sampled. The error bars represent one standard deviation.

was analyzed by optical detection (Fig. 3a) and sorted for further processing. Subsequent droplets of analyte with different concentrations ($4\times$ and $8\times$) followed a similar protocol except the droplet containing fluorescein was mixed with two, three, or four droplets of diluent respectively (Fig. 3b). Note that this type of process, which includes on-demand droplet generation and mixing to create different droplets of different concentration of analytes was only made possible with the integration of digital microfluidics. Such operations were not possible with typical droplet microfluidic platforms unless we increase the number of inlets and injectors or reinject droplets into the device.⁴⁴ The devices used in this experiment were done in droplet-in-channels with minimal inlets, which allowed for a maximum $8\times$ dilution of stock analyte. In

the future, more dilutions could be implemented or mixing different types of analytes could be implemented by using these devices.

Fig. 3c summarizes the results from the dilution series experiment with fluorescein. The emitted fluorescence from the droplet was detected by the spectrometer which outputted arbitrary units proportional to the emitted fluorescence of the droplet. As shown in Fig. 3c, the yellow curve depicts droplets that have minimal emitted fluorescence (*i.e.* droplets of diluent without fluorescein). The blue curve shows peaks that represent the fluorescence intensity for different concentrations of fluorescein and a baseline signal (close to zero) which represents the oil phase with no fluorescein. As expected, the highest fluorescein concentration (1 mM)

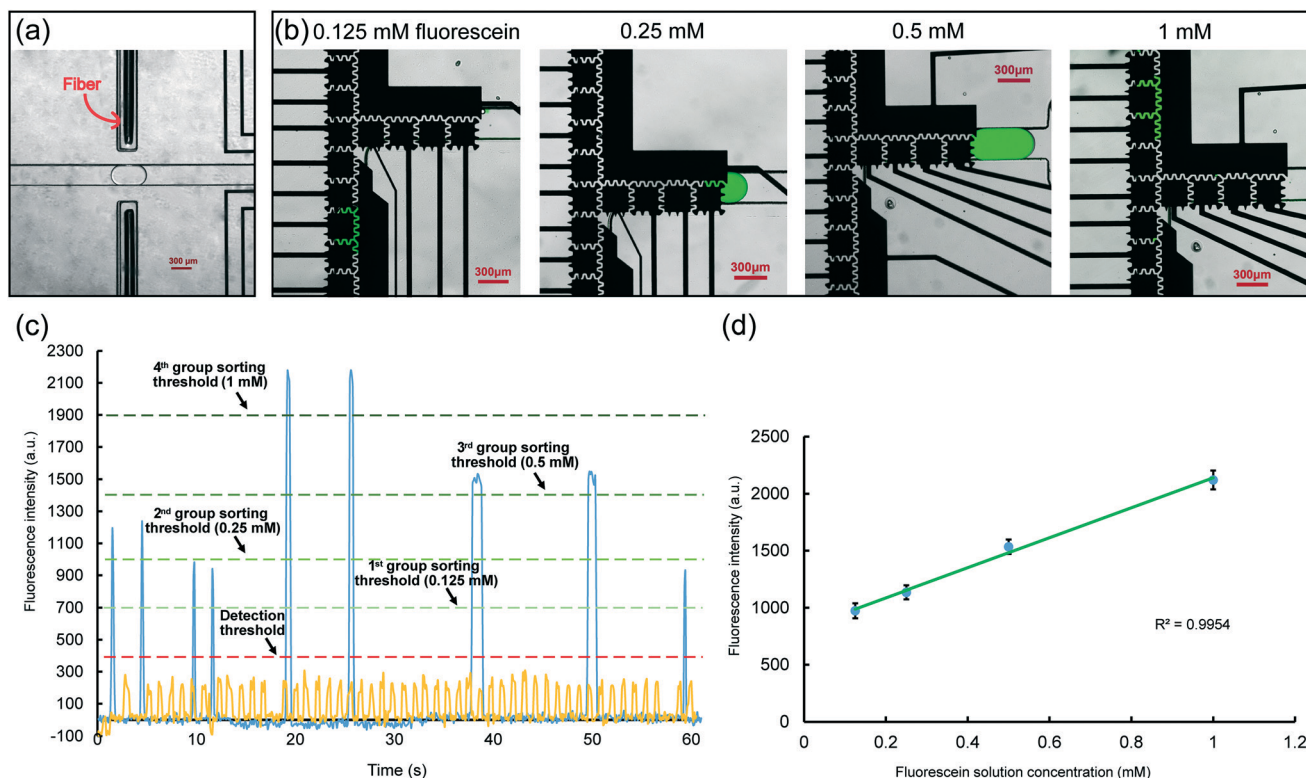


Fig. 3 On-chip calibration. (a) Image of the detection region on the ID2M device. (b) Images of droplets containing fluorescein at four different concentrations (0.125, 0.25, 0.5, and 1 mM) being sorted into a respective channel. (c) Time series during a sort showing the fluorescence signal (blue) for four concentrations of fluorescein and for droplets with only diluent (*i.e.* no fluorescein, yellow). Each droplet containing fluorescein is sorted by their threshold fluorescence intensity values (green dashed lines). (d) A calibration curve showing the fluorescence as a function of fluorescein concentration. The average fluorescence values were used to create the threshold values for sorting. Error bars are ± 1 S.D.

showed the highest signal with a sorting threshold ~ 1900 arbitrary units and the lower fluorescein concentration (0.125 mM) showed the lowest signal with a threshold of ~ 700 . A calibration curve ($N = 10$) was generated by plotting the ratio of analyte peak intensity as a function of analyte concentration (Fig. 3d). The precision in each measurement (RSD = 3.2%, 4.6%, 7.5%, and 10.7% for the stock, 2 \times , 4 \times , and 8 \times dilution, respectively) and the correlation coefficient ($R^2 = 0.99$) demonstrates that the method is reproducible and linear. Furthermore, we measured the sorting efficiency by sorting positive-fluorescein (1 mM) *vs.* negative-fluorescein droplets and obtained $\sim 96\%$ efficiency for positive (*i.e.* fluorescent) droplets which is similar to other reported sorting efficiencies.⁶²

ID2M application – effect of ionic liquid on yeast mutants

As an application of this work, we examined the effects of ionic liquid on wild-type and mutant yeast cells. Ionic liquid has been used as a promising pretreatment method for breaking down polysaccharides from typical feedstocks (*e.g.*, lignin) for sustainable production of renewable biofuels.^{63,64} Typically, there has been a wide range of available ILs that are suitable for effectively breaking down the required biomass.^{65,66} However, a major disadvantage with typical ILs (es-

pecially imidazolium ILs) is their inherent microbial toxicity which can either arrest growth of microbial cells, like *E. coli* or *S. cerevisiae*, or inhibit biofuel-related enzymes which can reduce the overall yield of biofuel production.^{67,68} Hence, there is much interest in investigating the mechanisms of tolerance for microbes to different levels of IL.

Here, we compare the effects of IL on wild-type and mutant yeast cells and show the ability to interrogate each cell type with different IL concentrations and to sort cells based on their growth differences. To our knowledge, this is the first time that microbes have been cultured, mixed with ionic liquid, and sorted based on multiple conditions (*i.e.* not binary). As a first step, we created a random mutant library (*via* ethyl methylsulfonate treatment) and verified their growth rates under IL conditions (Fig. 4a). We chose three types of yeast cells: wild-type and two best performing IL tolerant mutants and cultured them with and without 100 mM ionic liquid. As shown in Fig. 4b, the mutant cells showed faster rates (~ 2.2 and ~ 2.3 cell per hour for mutant #1 and mutant #2, respectively) compared to the wild-type cells (~ 0 cell per hour) in ionic liquid. In fact, the wild-type cells exhibited virtually no detectable growth in ionic liquid conditions. When cultured without ionic liquid, the wild type cells showed faster rates than both mutant cells (~ 3.4 and 3.7 cell per hour for the mutants and ~ 3.8 cell per hour for the wild-

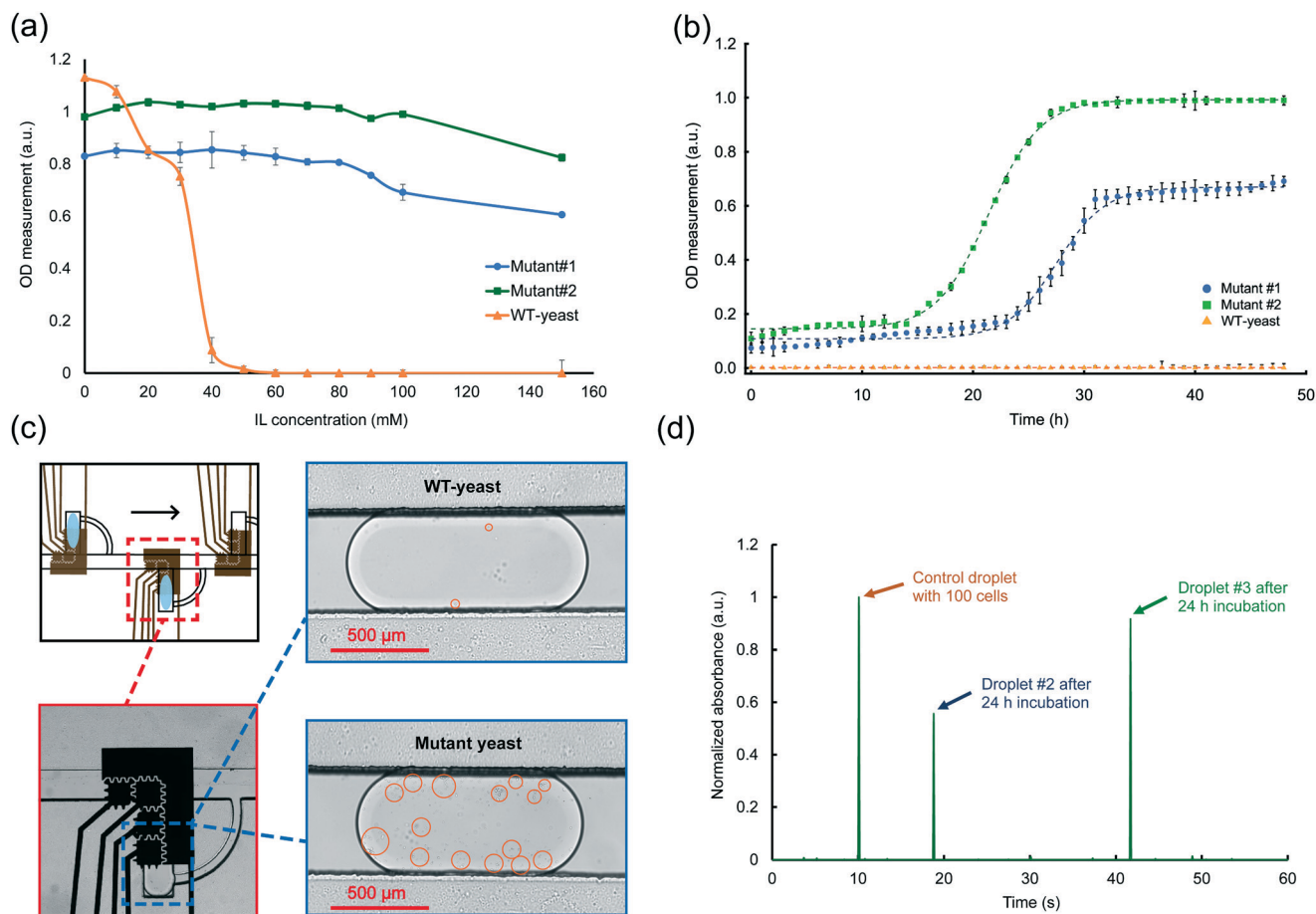


Fig. 4 ID2M application – effect of ionic liquid on mutant yeast cells. (a) OD measurements as a function of ionic liquid concentrations for wild-type and two mutant yeast cells after 24 h incubation and at 30 °C. (b) Growth curves for the wild-type and mutant yeast cells in 100 mM ionic liquid. (c) Pictures of wild-type and mutant yeast cells cultured in incubation regions on the device for 24 h confirming the differences between two cell lines. Cells are highlighted (circled regions) inside the droplet. (d) Raw data collected directly from the spectrometer showing the differences between the absorbance signals of droplets containing mutant and wild-type yeast.

type). The mechanisms of ionic liquid tolerance are still under debate, but we hypothesize that the location of the mutations in the yeast are in areas that are related to efflux pumps (*i.e.* to bring IL in-and-out of the cells)⁶⁹ and to transcriptional regulators that are related to stabilizing stress response.⁷⁰ Clearly, more work is required to determine the genotype location of the mutations (*i.e.* single-cell sequencing),⁷¹ but this experiment confirmed that we are capable of obtaining three different strains that will be used to show the utility of our device.

After selecting mutant phenotypes, we implemented the yeast mutant library screening protocol on our ID2M device. Fig. S6† shows the workflow for sorting different types yeast cells, starting with Poisson encapsulation of single cells in droplets to ensure that each droplet only contains a single type of cell. The single cell droplet is pressure-driven in the main channel until it reaches the mixing area. In this area, the droplet is actuated away from the main channel and into the mixing channel where it will merge and mix with a droplet of 200 mM IL, generated by the on-demand T-channel configuration. Next the droplet containing a sin-

gle cell in IL is actuated to the main channel and pressure-driven to the incubation channel. Upon arriving at the incubation region, the droplet is stored in one of the four incubation regions. After 24 h, the droplet was analyzed by absorbance and sorted by their cell density (*i.e.* cell number). Fig. 4c shows droplets that contained wild-type and mutant-type yeast cells with 100 mM IL. Mutant-type cells showed significant difference in the cell density compared to wild-type cells which are matching the growth rate results. On this device, we have integrated four steps (single cell encapsulation, mixing with IL, incubation, and sorting) that are required to screen for yeast mutants in IL. The integration of electrodes has provided several advantages in terms of droplet control: (1) the on-demand droplet generator can be activated at any time to generate a droplet of IL without the manipulation of flow rates, (2) merging and mixing droplets are controlled operations by the user (or automated sequences) and eliminates the requirement to optimize the time on when to add reagents to the droplets,⁴⁴ (3) droplets can be individually incubated in the side channels and accessed in any particular order (*i.e.* non-serial droplet

manipulation), and (4) droplets can be sorted based on a multi-dimensional space and not only on high-low producers.⁶ Here, the sorting is based on absorbance and the droplets containing cells are sorted based on two OD levels (Fig. 4d). As shown, the droplets containing mutant cells show peaks at ~ 0.6 and ~ 1 OD after 24 h incubation. Using these values, droplets in IL can be sorted by three cell types: wild type, mutant 1, and mutant 2. The absorbance signals generated from the mutants (representing the cell density) increases in IL while the signal for wild-type cells is similar to the signal of the oil phase (~ 0.04 – 0.07 ; see ESI† Fig. S7 for oil signal). In practice, the absorbance of the droplet is greater than that of the oil at higher cell densities (>20 cells) and similar to oil at low cell densities (<5 cells). Indeed, sensitivity of the signals depend on fiber alignment and background lighting which in our case we measure to be $<0.5\%$. We propose that improvement on the optical setup⁷² or device fabrication⁷³ can increase the sensitivity of our design and expanding the range of cell densities being observed. The method reported here enables a wide variety of droplet operations that is typically not possible with droplet or digital microfluidic systems – encapsulation, mixing (to generate different ionic liquid concentrations), culture and incubation, and n-ary sorting. Together the new methods described here may be particularly useful for high-throughput applications that require a creation of different drug concentrations or clonal libraries and sorting them at multiple levels.

Conclusion

We have developed an integrated droplet-digital microfluidic (ID2M) system that uses a combination of pressure- and electrical-based methods for the manipulation of droplets on chip. In this new method, four enhanced fluidic operations were created. First, droplets are generated by on-demand T-junction droplet generators (along with traditional flow-focusing techniques) which could generate a wide range of droplet volumes by tuning only the oil flow rate. Secondly, droplets were actuated to a mixing region that enabled merging with other droplets to form a dilution series of droplets. Third, after mixing, droplets could be trapped and incubated for several days simply by activating electrodes to guide the droplet into incubation traps. Lastly, this design included four channels (*i.e.* n-ary) for sorting droplets that contained different concentrations or constituents using fluorescence or absorbance. We showed the utility of this microfluidic device by studying the effects of ionic liquid on wild-type and mutant yeast cells. Using the four controlled fluidic steps, we were able to sort the cells into different fractions based on absorbance that can be analyzed downstream. We hypothesize that this system will be useful for those who are developing high-throughput screening platforms for single-cell analysis or directed evolution applications.

Author contributions

F. A. and S. C. C. S. designed the experiments. F. A. fabricated the ID2M devices, integrated the device with the automation and detection setup. F. A. performed all proof of concept experiments and constructed a fluorescein standard curve on chip with the help of K. S. and P. Q. N. V. wrote the software to operate the experiments on device. F. A. and K. S. carried out the mutagenesis and generated IL-resistant strains. F. A. performed the yeast cells n-ary sorting on chip and analysed the data with S. C. C. S., F. A. and S. C. C. S. wrote the paper, and all authors reviewed the final version of the manuscript before submission.

Conflicts of interest

The authors declare no conflict of interest.

Acknowledgements

We thank Vincent Martin's laboratory for donating BY4741 yeast strains and the Centre of Applied Synthetic Biology (CASB) for their technical support, Zahra Ahmadi for video editing, and Jess Sustarich for initial discussions. We thank the Natural Sciences and Engineering Research Council (NSERC), the Fonds de Recherche Nature et technologies (FRQNT), and the Canadian Foundation of Innovation (CFI) for funding. F. A. and K. S. thank Concordia University department of Electrical and Computer Engineering for FRS Funding. P. Q. N. V. thanks NSERC.

References

- 1 J. J. Agresti, E. Antipov, A. R. Abate, K. Ahn, A. C. Rowat, J. C. Baret, M. Marquez, A. M. Klibanov, A. D. Griffiths and D. A. Weitz, *Proc. Natl. Acad. Sci. U. S. A.*, 2010, **107**, 4004–4009.
- 2 M. T. Guo, A. Rotem, J. A. Heyman and D. A. Weitz, *Lab Chip*, 2012, **12**, 2146–2155.
- 3 T. Schneider, J. Kreutz and D. T. Chiu, *Anal. Chem.*, 2013, **85**, 3476–3482.
- 4 H. N. Joensson and H. A. Svahn, *Angew. Chem., Int. Ed.*, 2012, **51**, 12176–12192.
- 5 L. Mazutis, J. Gilbert, W. L. Ung, D. A. Weitz, A. D. Griffiths and J. A. Heyman, *Nat. Protoc.*, 2013, **8**, 870–891.
- 6 J. Abatemarco, M. F. Sarhan, J. M. Wagner, J. L. Lin, L. Q. Liu, W. Hassouneh, S. F. Yuan, H. S. Alper and A. R. Abate, *Nat. Commun.*, 2017, **8**, 332.
- 7 F. Gielen, R. Hours, S. Emond, M. Fischlechner, U. Schell and F. Hollfelder, *Proc. Natl. Acad. Sci. U. S. A.*, 2016, **113**, E7383–E7389.
- 8 K. Ahn, C. Kerbage, T. P. Hunt, R. M. Westervelt, D. R. Link and D. A. Weitz, *Appl. Phys. Lett.*, 2006, **88**, 024104.
- 9 K. Zhang, Q. L. Liang, S. Ma, X. A. Mu, P. Hu, Y. M. Wang and G. A. Luo, *Lab Chip*, 2009, **9**, 2992–2999.
- 10 V. Miralles, A. Huerre, H. Williams, B. Fournie and M. C. Jullien, *Lab Chip*, 2015, **15**, 2133–2139.

- 11 T. Franke, A. R. Abate, D. A. Weitz and A. Wixforth, *Lab Chip*, 2009, 9, 2625–2627.
- 12 H. D. Xi, H. Zheng, W. Guo, A. M. Ganan-Calvo, Y. Ai, C. W. Tsao, J. Zhou, W. Li, Y. Huang, N. T. Nguyen and S. H. Tan, *Lab Chip*, 2017, 17, 751–771.
- 13 K. Choi, A. H. Ng, R. Fobel and A. R. Wheeler, *Annu. Rev. Anal. Chem.*, 2012, 5, 413–440.
- 14 M. J. Jebrail, M. S. Bartsch and K. D. Patel, *Lab Chip*, 2012, 12, 2452–2463.
- 15 O. D. Velev, B. G. Prevo and K. H. Bhatt, *Nature*, 2003, 426, 515–516.
- 16 C. Chen, S. P. Zhang, Z. Mao, N. Nama, Y. Gu, P. H. Huang, Y. Jing, X. Guo, F. Costanzo and T. J. Huang, *Lab Chip*, 2018, 18, 3645–3654.
- 17 S. P. Zhang, J. Lata, C. Chen, J. Mai, F. Guo, Z. Tian, L. Ren, Z. Mao, P. H. Huang, P. Li, S. Yang and T. J. Huang, *Nat. Commun.*, 2018, 9, 2928.
- 18 I. Barbulovic-Nad, H. Yang, P. S. Park and A. R. Wheeler, *Lab Chip*, 2008, 8, 519–526.
- 19 N. Vergauwe, D. Witters, F. Ceyskens, S. Vermeir, B. Verbruggen, R. Puers and J. Lammertyn, *J. Micromech. Microeng.*, 2011, 21, 5.
- 20 M. C. Husser, P. Q. N. Vo, H. Sinha, F. Ahmadi and S. C. C. Shih, *ACS Synth. Biol.*, 2018, 7, 933–944.
- 21 S. C. C. Shih, G. Goyal, P. W. Kim, N. Koutsoubelis, J. D. Keasling, P. D. Adams, N. J. Hillson and A. K. Singh, *ACS Synth. Biol.*, 2015, 4, 1151–1164.
- 22 D. G. Rackus, M. D. Dryden, J. Lamanna, A. Zaragoza, B. Lam, S. O. Kelley and A. R. Wheeler, *Lab Chip*, 2015, 15, 3776–3784.
- 23 A. H. C. Ng, R. Fobel, C. Fobel, J. Lamanna, D. G. Rackus, A. Summers, C. Dixon, M. D. M. Dryden, C. Lam, M. Ho, N. S. Mufti, V. Lee, M. A. M. Asri, E. A. Sykes, M. D. Chamberlain, R. Joseph, M. Ope, H. M. Scobie, A. Knipes, P. A. Rota, N. Marano, P. M. Chege, M. Njuguna, R. Nzunza, N. Kisangau, J. Kiogora, M. Karuingi, J. W. Burton, P. Borus, E. Lam and A. R. Wheeler, *Sci. Transl. Med.*, 2018, 10, 438.
- 24 M. Abdelgawad, S. L. Freire, H. Yang and A. R. Wheeler, *Lab Chip*, 2008, 8, 672–677.
- 25 C. G. Cooney, C.-Y. Chen, M. R. Emerling, A. Nadim and J. D. Sterling, *Microfluid. Nanofluid.*, 2006, 2, 435–446.
- 26 M. Abdelgawad, M. W. Watson and A. R. Wheeler, *Lab Chip*, 2009, 9, 1046–1051.
- 27 M. W. Watson, M. J. Jebrail and A. R. Wheeler, *Anal. Chem.*, 2010, 82, 6680–6686.
- 28 S. C. Shih, P. C. Gach, J. Sustarich, B. A. Simmons, P. D. Adams, S. Singh and A. K. Singh, *Lab Chip*, 2015, 15, 225–236.
- 29 D. Huh, A. H. Tkaczyk, J. H. Bahng, Y. Chang, H. H. Wei, J. B. Grotberg, C. J. Kim, K. Kurabayashi and S. Takayama, *J. Am. Chem. Soc.*, 2003, 125, 14678–14679.
- 30 H. Gu, F. Malloggi, S. A. Vanapalli and F. Mugele, *Appl. Phys. Lett.*, 2008, 93, 183507.
- 31 F. Malloggi, H. Gu, A. G. Banpurkar, S. A. Vanapalli and F. Mugele, *Eur. Phys. J. E: Soft Matter Biol. Phys.*, 2008, 26, 91–96.
- 32 R. de Ruiter, A. M. Pit, V. M. de Oliveira, M. H. G. Duits, D. van den Ende and F. Mugele, *Lab Chip*, 2014, 14, 883–891.
- 33 A. M. Pit, R. de Ruiter, A. Kumar, D. Wijnperle, M. H. G. Duits and F. Mugele, *Biomicrofluidics*, 2015, 9(4), 044116.
- 34 M. G. Simon, R. Lin, J. S. Fisher and A. P. Lee, *Biomicrofluidics*, 2012, 6, 14110–1411013.
- 35 B. O'Donovan, D. J. Eastburn and A. R. Abate, *Lab Chip*, 2012, 12, 4029–4032.
- 36 H. Song and R. F. Ismagilov, *J. Am. Chem. Soc.*, 2003, 125, 14613–14619.
- 37 L. Frenz, K. Blank, E. Brouzes and A. D. Griffiths, *Lab Chip*, 2009, 9, 1344–1348.
- 38 J. Clausell-Tormos, D. Lieber, J. C. Baret, A. El-Harrak, O. J. Miller, L. Frenz, J. Blouwolf, K. J. Humphry, S. Koster, H. Duan, C. Holtze, D. A. Weitz, A. D. Griffiths and C. A. Merten, *Chem. Biol.*, 2008, 15, 427–437.
- 39 S. Koster, F. E. Angile, H. Duan, J. J. Agresti, A. Wintner, C. Schmitz, A. C. Rowat, C. A. Merten, D. Pisignano, A. D. Griffiths and D. A. Weitz, *Lab Chip*, 2008, 8, 1110–1115.
- 40 P. Q. N. Vo, M. C. Husser, F. Ahmadi, H. Sinha and S. C. C. Shih, *Lab Chip*, 2017, 17, 3437–3446.
- 41 F. Winston, *Curr. Protoc. Mol. Biol.*, 2008, 82, 13.13B.11–13.13B.15.
- 42 M. Chabert, K. D. Dorfman and J. L. Viovy, *Electrophoresis*, 2005, 26, 3706–3715.
- 43 K. Ahn, J. Agresti, H. Chong, M. Marquez and D. A. Weitz, *Appl. Phys. Lett.*, 2006, 88, 264105.
- 44 A. R. Abate, T. Hung, P. Mary, J. J. Agresti and D. A. Weitz, *Proc. Natl. Acad. Sci. U. S. A.*, 2010, 107, 19163–19166.
- 45 A. Banerjee, E. Kreit, Y. G. Liu, J. Heikenfeld and I. Papautsky, *Lab Chip*, 2012, 12, 758–764.
- 46 M. Abdelgawad, P. Park and A. R. Wheeler, *J. Appl. Phys.*, 2009, 105, 094506.
- 47 P. Y. Paik, V. K. Pamula and K. Chakrabarty, *IEEE Transactions on Very Large Scale Integration (VLSI) Systems*, 2008, 16, 432–443.
- 48 U. C. Yi and C. J. Kim, *J. Micromech. Microeng.*, 2006, 16, 2053–2059.
- 49 R. Yang, S. A. Soper and W. Wang, *Sens. Actuators, A*, 2007, 135, 625–636.
- 50 Y. Ren, S.-H. Huang, S. Mosser, O. M. Heuschkel, A. Bertsch, C. P. Fraering, J. J.-J. Chen and P. Renaud, *Micromachines*, 2015, 6(12), 1923–1934.
- 51 N. Yanagisawa and T. Higashiyama, *Biomicrofluidics*, 2018, 12(2), 024113.
- 52 W. W. Cui, M. L. Zhang, X. X. Duan, W. Pang, D. H. Zhang and H. Zhang, *Micromachines*, 2015, 6, 778–789.
- 53 S. S. Bithi and S. A. Vanapalli, *Biomicrofluidics*, 2010, 4, 044110.
- 54 J. C. Baret, O. J. Miller, V. Taly, M. Ryckelynck, A. El-Harrak, L. Frenz, C. Rick, M. L. Samuels, J. B. Hutchison, J. J. Agresti, D. R. Link, D. A. Weitz and A. D. Griffiths, *Lab Chip*, 2009, 9, 1850–1858.
- 55 S. X. Li, X. Y. Ding, F. Guo, Y. C. Chen, M. I. Lapsley, S. C. S. Lin, L. Wang, J. P. McCoy, C. E. Cameron and T. J. Huang, *Anal. Chem.*, 2013, 85, 5468–5474.
- 56 D. H. Yoon, J. Ito, T. Sekiguchi and S. Shoji, *Micromachines*, 2013, 4, 197–205.

- 57 E. Fradet, C. McDougall, P. Abbyad, R. Dangla, D. McGloin and C. N. Baroud, *Lab Chip*, 2011, **11**, 4228–4234.
- 58 Y. G. Liu, A. Banerjee and I. Papautsky, *Microfluid. Nanofluid.*, 2014, **17**, 295–303.
- 59 S. L. Anna, N. Bontoux and H. A. Stone, *Appl. Phys. Lett.*, 2003, **82**, 364–366.
- 60 T. Ward, M. Faivre, M. Abkarian and H. A. Stone, *Electrophoresis*, 2005, **26**, 3716–3724.
- 61 P. Paik, V. K. Pamula and R. B. Fair, *Lab Chip*, 2003, **3**, 253–259.
- 62 A. Sciambi and A. R. Abate, *Lab Chip*, 2015, **15**, 47–51.
- 63 C.-Z. Liu, F. Wang, A. R. Stiles and C. Guo, *Appl. Energy*, 2012, **92**, 406–414.
- 64 H. W. Blanch, B. A. Simmons and D. Klein-Marcuschamer, *Biotechnol. J.*, 2011, **6**, 1086–1102.
- 65 J. Sun, D. Liu, R. P. Young, A. G. Cruz, N. G. Isern, T. Schuerg, J. R. Cort, B. A. Simmons and S. Singh, *ChemSusChem*, 2018, **11**, 781–792.
- 66 M. Ouellet, S. Datta, D. C. Dibble, P. R. Tamrakar, P. I. Benke, C. Li, S. Singh, K. L. Sale, P. D. Adams, J. D. Keasling, B. A. Simmons, B. M. Holmes and A. Mukhopadhyay, *Green Chem.*, 2011, **13**, 2743–2749.
- 67 J. I. Park, E. J. Steen, H. Burd, S. S. Evans, A. M. Redding-Johnson, T. Batth, P. I. Benke, P. D'Haeseleer, N. Sun, K. L. Sale, J. D. Keasling, T. S. Lee, C. J. Petzold, A. Mukhopadhyay, S. W. Singer, B. A. Simmons and J. M. Gladden, *PLoS One*, 2012, **7**, e37010.
- 68 Y. V. Nancharaiyah and A. J. Francis, *Bioresour. Technol.*, 2011, **102**, 6573–6578.
- 69 T. L. Ruegg, E. M. Kim, B. A. Simmons, J. D. Keasling, S. W. Singer, T. S. Lee and M. P. Thelen, *Nat. Commun.*, 2014, **5**, 3490.
- 70 M. Frederix, F. Mingardon, M. Hu, N. Sun, T. Pray, S. Singh, B. A. Simmons, J. D. Keasling and A. Mukhopadhyay, *Green Chem.*, 2016, **18**, 4189–4197.
- 71 H. S. Moon, K. Je, J. W. Min, D. Park, K. Y. Han, S. H. Shin, W. Y. Park, C. E. Yoo and S. H. Kim, *Lab Chip*, 2018, **18**, 775–784.
- 72 R. H. Cole, N. de Lange, Z. J. Gartner and A. R. Abate, *Lab Chip*, 2015, **15**, 2754–2758.
- 73 R. Blue and D. Uttamchandani, *J. Biophotonics*, 2016, **9**, 13–25.